



OPEN

A detailed investigation of dielectric-modulated dual-gate TMD FET based label-free biosensor via analytical modelling

Monika Kumari^{1,2}, Niraj Kumar Singh^{1,2} & Manodipan Sahoo^{1,2}✉

In this work, an analytical model is developed for DM-DG-TMD-FET- based Biosensor including Fringing-field effects. The Analytical model has been developed for two different Device structures, namely Device structure-1 (without a gate above the nano-cavity) and Device structure-2 (with a gate above the nano-cavity) based on modulation of the dielectric constant of biomolecules in the nano-cavity region. The proposed model has been validated against both numerical quantum simulation results with the help of a few fitting parameters and it also agrees with the 2-dimensional numeric simulator SILVACO TCAD used in this work. The presence/absence of biomolecules has been detected by the metric of threshold voltage sensitivity $S_{V_{th}}$ and drain current I_d for the neutral as well as charged biomolecules. Sensitivities of partially filled nano-cavities arising out of steric hindrance in both the biosensors are compared. Optimization of device dimensions has also been included in this work to enhance the sensitivity of the biosensors. It has been witnessed that the sensitivity of the proposed biosensor is $\sim 100\%$ higher in Device structure-1 for neutral biomolecules with dielectric constant $\kappa = 12$, when compared to Device structure-2 for fully filled cavities. Whereas for the charged biomolecules, Device structure-1 shows $\sim 50\%$ enhanced sensitivity than Device structure-2 for $N_f = -1 \times 10^{-12} \text{ C/cm}^2$. Device structure-1 demonstrates $\sim 120\%$ higher sensitivity than Device structure-2 with partially filled cavities (i.e. 66% filled cavity). Finally, benchmarking of the proposed biosensor is presented with contemporary, state-of-the-art biosensors and it is highlighted that MoS_2 FET-based biosensor emerges with a superior sensitivity of $S_{V_{th}} = 0.81 \text{ V}$ for $\kappa = 12$.

FET-based biosensors have been extensively investigated to detect a range of target biomolecules due to their superior sensitivity, swift label-free detection capabilities, low power consumption, compatibility with CMOS technology, and large scale production at a low cost. These factors have become more critical as the demand for ultrasensitive biosensors has risen in fields such as medicine, agriculture, defence, and environmental monitoring, among others¹⁻³. Among FET-based biosensors, Dielectric Modulated (DM) FETs have shown better sensitivity and are mostly preferred in the field of biosensing applications as the created nano-cavities provide sufficient volume and efficient conjugation of biomolecules which results in enhancement in sensitivity⁴. Choi et al. demonstrated the first DM-FET-based biosensor with nano-cavities for label-free detection of biomolecules². After that many dielectric-modulated FET-based biosensors have been reported with the enhancement in sensitivity⁵⁻⁹.

FET-based biosensors with 1-D Nanowires and CNTs as channel material have a significant advantage over label-based detection¹⁰ because they exhibit good electrostatics between biomolecules and the channel, resulting in increased sensitivity. However, synthesizing biosensors that meet all of these criteria at the same time has proven difficult, as 0-D and 1-D nanomaterials-based biosensors are difficult to fabricate on a large scale and have high production costs¹¹⁻¹³, limiting the practical feasibility of such structures.

Contrarily, tremendous progress has recently been made with Transition Metal Dichalcogenides (TMDs), one of the most intriguing 2-D semiconducting materials for next-generation biosensors. Because of their excellent electrostatic control, planar nature, high surface-to-volume ratio, superior charge sensitivity, and high electron mobility, among other advantage, TMDs hold a lot of promise for use as a channel in FET-based ultra-sensitive biosensors^{12,14}.

¹Department of Electronics Engineering, Indian Institute of Technology (Indian School of Mines), Dhanbad 826004, India. ²These authors contributed equally: Monika Kumari, Niraj Kumar Singh and Manodipan Sahoo. ✉email: manodipan@iitism.ac.in

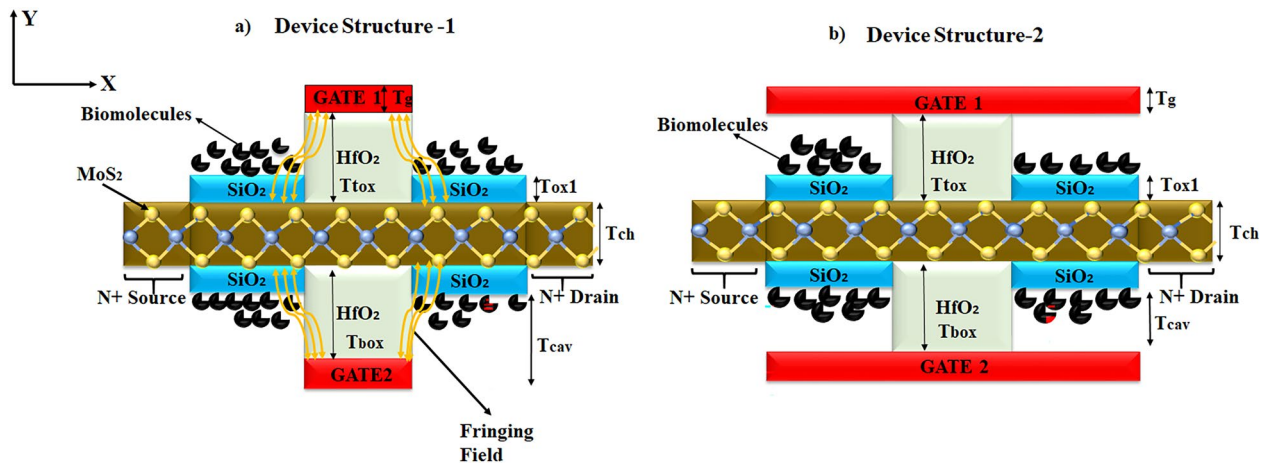


Figure 1. (a) Device structure-1 of dielectric-modulated, dual-gate, TMD FET (DM-DG-TMD-FET)-based Biosensor, and (b) Device structure-2 of DM-DG-TMD-FET-based biosensor.

Furthermore, due to their comparably weak interlayer connections, 2-D materials have a lower surface roughness than 3-D materials¹⁵. TMD materials unlike Graphene exhibit a band-gap that is essential for the operation of FET-based biosensors since the binding process at the interface between the channel and biomolecules modulates the carrier transport in 2-D layered materials¹⁶.

Moreover, in recent years the application of various 2-D layered materials like MoS_2 , WSe_2 and $MoSe_2$ in FET-based biosensors has become extremely promising. $MoSe_2$ has smaller band-gap than MoS_2 and WSe_2 but it exhibits larger reduced effective mass which is preferable for Tunnel FET-based applications^{17,18}. Whereas, WSe_2 -based biosensors exhibit higher linear-regime sensitivities in comparison with MoS_2 -based biosensors¹⁹. Because of the recent advances in the synthesis of MoS_2 sheets using CVD and liquid phase exfoliation techniques^{12,16}, as well as their excellent compatibility with commercial planar processes for large scale production^{15,20}, MoS_2 FET-based biosensors are widely investigated among TMD materials.

Sarkar et al. have reported detection of streptavidin using MoS_2 FET-based biosensor with HfO_2 as gate dielectric functionalized with biotin¹¹. Wang et al. have reported APTES functionalized MoS_2 nanosheet-based biosensor for the cancer marker protein detection²¹. Nam et al. have reported MoS_2 FET-based biosensor functionalized with $TNF-\alpha$ anti-bodies for sensing of $TNF-\alpha$ molecules²².

However, in order to further investigate 2-D material based FET in biosensing applications, an analytical I-V model that accounts for realistic circumstances when conjugating the biomolecules in the nano-cavities, which seem to be unavoidable during fabrication, is required. Unfortunately, little progress has been made in developing various analytical models for DM-TMD-FET-based biosensors. An I-V model has been developed by Rahman et al.²³ for single-sided cavity, MoS_2 -based biosensor. However, this model does not take into account fringing-field effects, which in sub-100 nm FETs cannot be disregarded. Furthermore, the author has investigated the effect on sensitivities when the nano-cavities are filled completely, which is practically impossible.

Main contributions of this work can be summarized as: an analytical model of DM-TMD-FET-based biosensor has been developed including several design parameters like nano-cavity thickness, dielectric constant and charge of biomolecules. The veracity of the model has been verified with experimental data²⁴ and 2-D numeric simulator SILVACO TCAD²⁵. Two device structures namely, Device structure-1 (without gate above the nano-cavity) and Device structure-2 (with gate above the nano-cavity) have been investigated incorporating fringing-field effects in the model and its effect on the characteristics of the biosensors has been analyzed. Sensitivity metrics such as threshold voltage V_{th} , shift in threshold voltage ΔV_{th} and drain current are estimated for neutral biomolecules as well as charged biomolecules. Partially filled nano-cavities with different filling factors have also been considered in this work and the analytical model has been developed to incorporate this. The effect of steric hindrance including concave, convex, decreasing, and increasing step profiles in the nano-cavity has been considered and the impact of these profiles on the sensitivity has been observed.

Device structure

Figure 1a,b show the schematic of the proposed monolayer TMD-FET-based biosensor without gate over cavity and with gate over cavity.

An equivalent capacitance model of the device structure-1 and 2 has also been drawn in Fig. 2. Here, x is the channel direction and, y is perpendicular to the channel. The channel region is divided into three parts, regions at both the source (L_1) and the drain side (L_3) work as cavity, where biomolecules can be immobilized, region beneath the high- κ gate oxide is the overlap region, (L_2). A SiO_2 layer having thickness 1 nm is taken in the cavity regions, as illustrated in Fig. 1, which acts as an adhesion layer for the biomolecules³. Since, MoS_2 -based biosensor has been widely explored^{26,27} in the recent years, it has been utilized as a channel material for performing various analysis in this work. Other TMD materials like, WSe_2 and $MoSe_2$ can also be deployed as channel materials²⁸. TMD-FET-based biosensor under consideration consists of a monolayer p-doped MoS_2 channel sandwiched between the top and the bottom HfO_2 layer. Al is used as top and bottom gates. Highly n-doped monolayer MoS_2

Symbol	Parameters	Range
L_{ch}	Length of the channel	100 nm
L_1, L_3	Length of the nano-cavity	30 nm
L_g	Length of gates for device structure	60 nm
T_{tox}	Thickness of the front gate oxide	10 nm
T_{box}	Thickness of the back gate oxide	10 nm to 200 nm
T_{cav}	Thickness of the nano-cavity	10 nm
$W.F$	Work function of gates	4.1 eV
N_{ch}	Channel doping	10^{18} cm^{-2}
N_{sd}	Source and drain doping	10^{20} cm^{-2}

Table 1. Device parameters of the proposed structure.

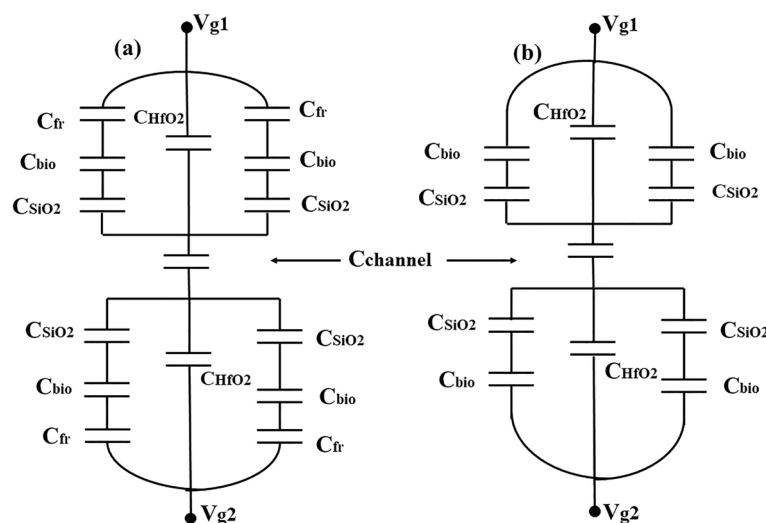


Figure 2. Equivalent Capacitance Model for (a) Device structure-1, (b) Device structure-2.

has been used in the source and the drain regions. The channel has a thickness and length of 0.7 nm¹⁹ and 60 nm respectively. On the source and drain sides, the cavity is 20 nm long, respectively. The top and bottom oxide layers are each 10 nm thick. The remaining model parameters are listed in Table 1. A tentative fabrication process^{20,27,29} of the proposed TMD FET-based biosensor has been depicted in Fig. 3.

Results and discussions

The characteristics of the DM-DG-TMD-FET-based biosensor for neutral and charged biomolecules are discussed in this section. The sensitivity of the biosensor is measured in terms of threshold voltage (V_{th}), variation in threshold voltage (ΔV_{th}) and drain current (I_{ds}).

The proposed model is validated with the experimental I-V characteristics of monolayer WSe_2 by Fang et al.²⁴, quantum simulation results obtained by Rahman et al.²³ and with two dimensional numerical simulator Silvaco TCAD²⁵. Exactly same sets of the device and material parameters are utilized to validate our proposed model with the simulator. Figure 4 depicts the I-V characteristics of the DM-DG-TMD-FET-based biosensor obtained from the model along with the experimental results reported by Fang et al.²⁴. Figure 5 shows the surface potential of DM-DG-TMD FET-based biosensor, which has been validated with self consistent NEGF simulation results of²³. Drain current and surface potential shows a close match with the results from²⁴ and²³. Little discrepancy exists as a result of the various environmental set-up.

Impact of neutral biomolecules and charged biomolecules on sensitivity. In this section, we have explored the impact of neutral biomolecules and charged biomolecules on the surface potential, threshold voltage V_{th} and drain current of the proposed two structures of DM-DG-TMD-FET-based biosensor. Figure 6a shows the bending in surface potential when neutral biomolecules get immobilized in the cavity for the proposed DM-DG-TMD-FET-based biosensor, structure-1. In Device structure-1, there is no gate over nano-cavity so the effect of flat band voltage V_{fb} is negligible and fringing capacitance plays a dominant role by influencing the surface potential. Deviation in the surface potential profile is clearly observed under the nano-cavity region, whereas, no deformation of the potential profile is observed in the region without a nano-cavity.

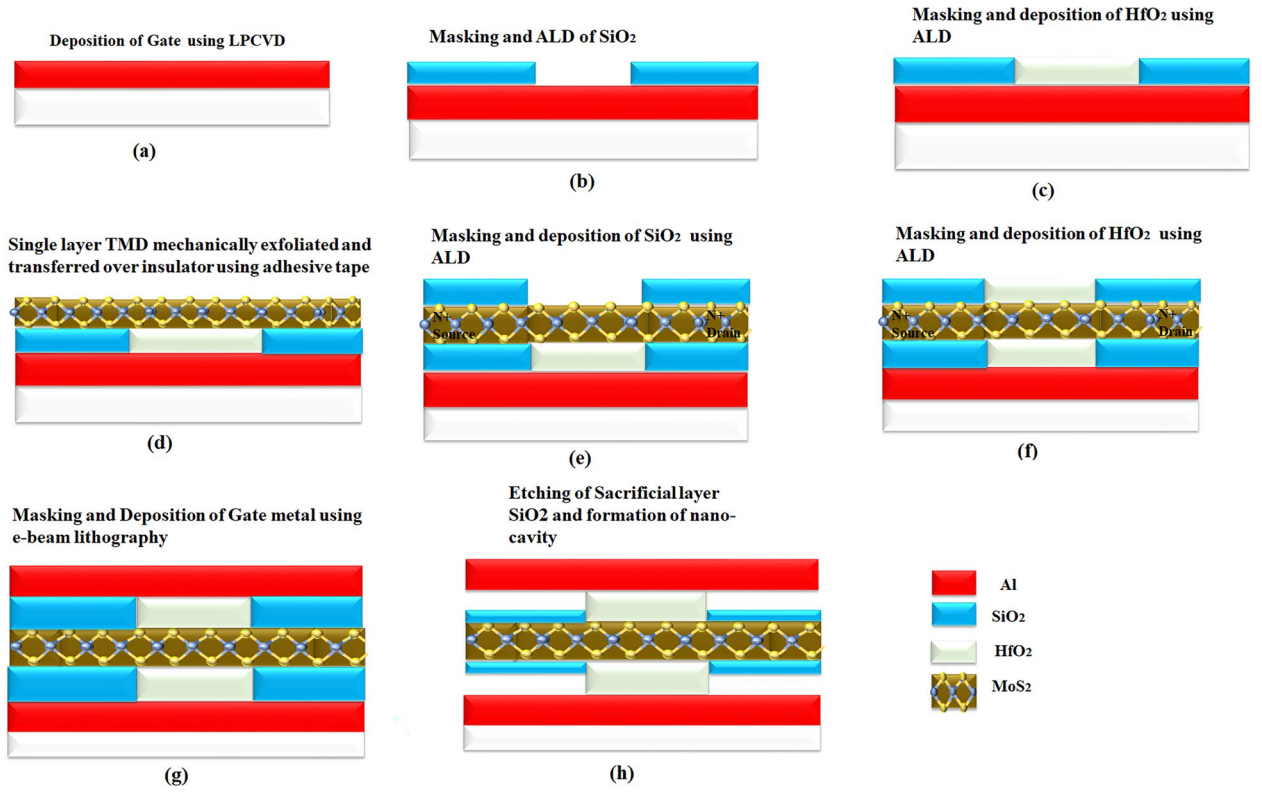


Figure 3. Proposed fabrication process of the DM-DG-TMD-FET-based biosensor.

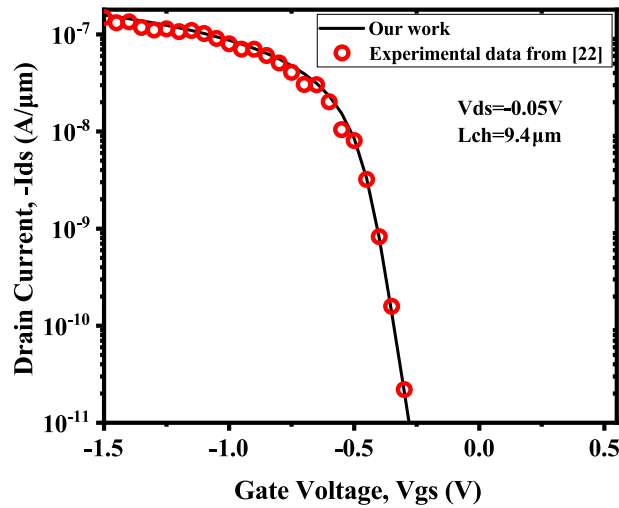


Figure 4. Drain current, (I_{ds}) versus Gate to source bias, (V_{gs}) for back-gate, (V_{gb}) – 40 V and drain to source bias, $V_{ds} = -0.05$ V with channel-length, $L_{ch} = 9.4$ nm, front and back gate oxides are ZrO_2 $T_{tox} = 17.5$ nm, $k_{tox} = 12.5$ and SiO_2 ($T_{box} = 270$ nm, $k_{box} = 3.9$) respectively.

When the cavity is empty i.e filled with air ($\kappa = 1$) the gate capacitance is low and the flat band voltage V_{fb} in the cavity part is negligible so the voltage requirement will be more for the electrons to cross the source-channel barrier which is evident from (1). The V_{th} of a MOSFET can be expressed as³⁰

$$V_{th} = V_{fb} + 2\phi_b + \frac{q(\pm N_f)}{C_{eff}} \tag{1}$$

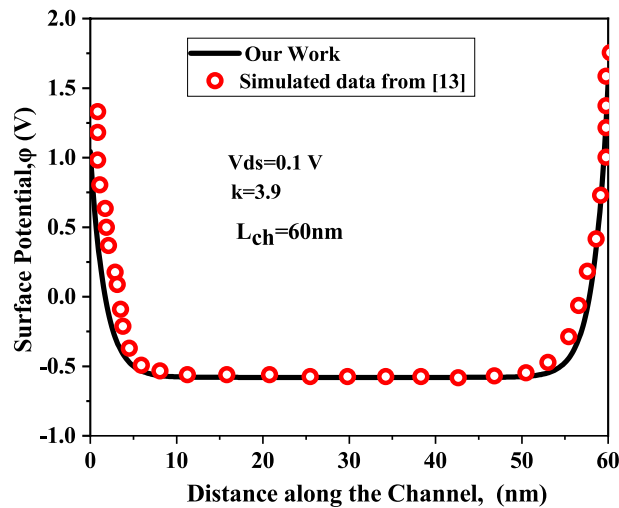


Figure 5. Surface potential calculated using our proposed model vs. quantum simulated data of²³ for $V_{gs} = 1$ V.

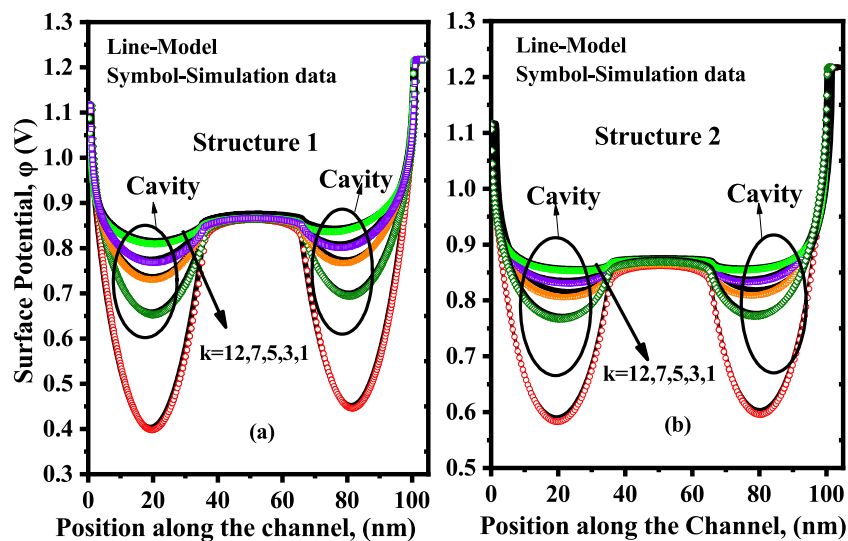


Figure 6. Surface potential of the proposed DM-DG-TMD-FET-based biosensor for (a) Device structure-1 and, (b) Device structure-2 with different dielectric constants ($\kappa = 1, 3, 5, 7, 12$) of biomolecules. ($V_{gs} = 0.1$ V, $V_{ds} = 0.1$ V $N_f = 0$).

Moreover, when the dielectric constant of the biomolecules increases, the effective gate capacitance rises along with fringing-field capacitance, changing the surface potential in the cavity region. Thus with an increase in the dielectric constant of biomolecules the fringing-field effects dominates and the surface potential barrier is reduced.

For the proposed Device structure-2, Fig. 6b illustrates the deformation in surface potential when neutral biomolecules get immobilised in the cavity. Since there is gate over cavity, fringing capacitance is not dominant in this case and the control of gate over channel is adequate, as the channel is p-type, there will be negative flat band voltage across the channel and the amount of threshold voltage for the electrons to cross the source channel barrier will be less. In this case also the surface potential barrier decreases with the increase in dielectric constants of the biomolecules but the reduction in barrier is more when compared to Device structure-1 because of the presence of gate control throughout the channel region and sufficient amount of flat band voltage V_{fb} .

When the target biomolecules are immobilized in the nano-cavities, device characteristics are modulated according to the quantity of target biomolecules. The threshold voltage V_{th} and change in threshold voltage $S_{V_{th}}$ are the most commonly utilised sensing metrics for evaluating the effectiveness of the biosensors among the different parameters that are affected by the target biomolecules.

It is evident from Fig. 7a,b, that the threshold voltage requirement for Device structure-1 is higher than that for Device structure-2, as the gate control over the channel in structure-1 is less so the V_{fb} is negligible in the cavity area and threshold voltage increases and due to the fringing effect there is more increase in threshold voltage. For Device structure-2 there is full gate control over the channel thus threshold voltage requirement is less. It is

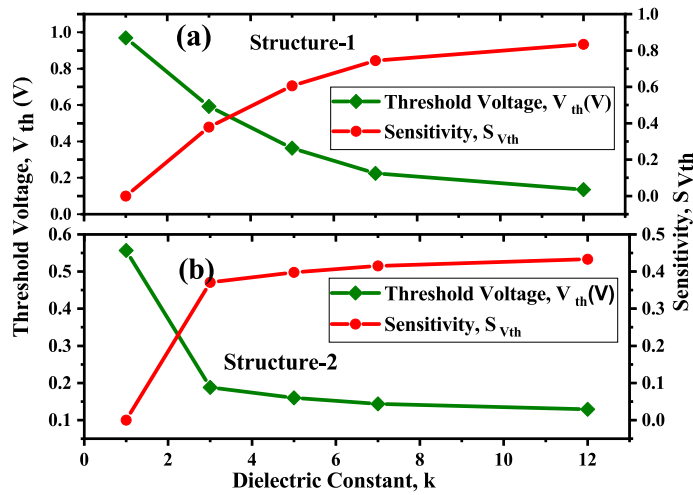


Figure 7. Threshold voltage and Sensitivity w.r.t to dielectric constant (κ) of biomolecules with for Device structure-1 and Device structure-2 ($V_{gs} = 1.2$ V, $\kappa = 5$, $N_f = 0$).

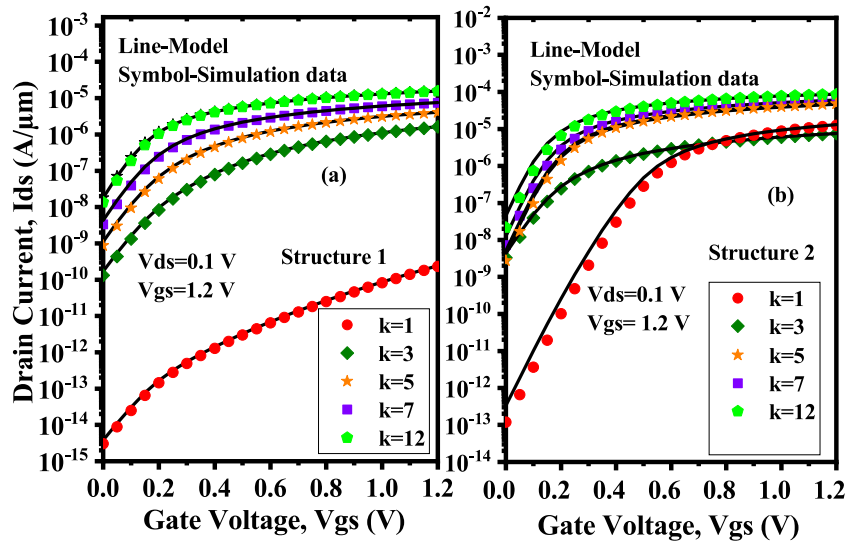


Figure 8. Variation in drain current w.r.t to gate bias for (a) Device structure-1 and (b) Device structure-2 ($V_{gs} = 1.2$ V, $V_{ds} = 0.1$ V, dielectric constants, $\kappa = 1, 3, 5, 7, 12$, $N_f = 0$).

also evident from Fig. 7a,b, that the threshold voltage decreases with the increasing κ . When the cavity is empty (i.e $\kappa = 1$), the threshold voltage achieved is high, i.e 0.969 V for structure-1 and and 0.569 V for structure-2.

Figure 7a,b plots the sensitivity of the proposed two structures of DM-DG-TMD-FET-based biosensors. The sensitivity of the biosensor is measured by a shift in threshold voltage (S_{vth}) before and after immobilization of the biomolecules in the nano-cavity region. Thereby, it can be defined as³¹

$$S_{vth} = \frac{V_{th}(\kappa = 1) - V_{th}(\kappa > 1)}{V_{th}(\kappa = 1)} \quad (2)$$

It can be observed that sensitivity of device structure-1 is $\sim 100\%$ more than the sensitivity of device structure-2. As in the proposed biosensor structure-1, fringing capacitance dominates the total capacitance which leads to increase the threshold voltage as well as overall enhancement in the sensitivity.

Figure 8a shows the drain current variation when neutral biomolecules are conjugated in the nano-cavity region of the proposed Device structure-1. The OFF current of the device is minimum when the cavity is empty and it increases when the dielectric constant κ in the cavity region increases, whereas, there is slightly increment in ON current. Now, comparing Device structure-2 Fig. 8b to Device structure-1, the ON and OFF current increases as the dielectric constants κ increase. The variation in OFF current is greater than the variation in ON current because FETs conduct extremely low current in the subthreshold regime, so a smaller change in potential

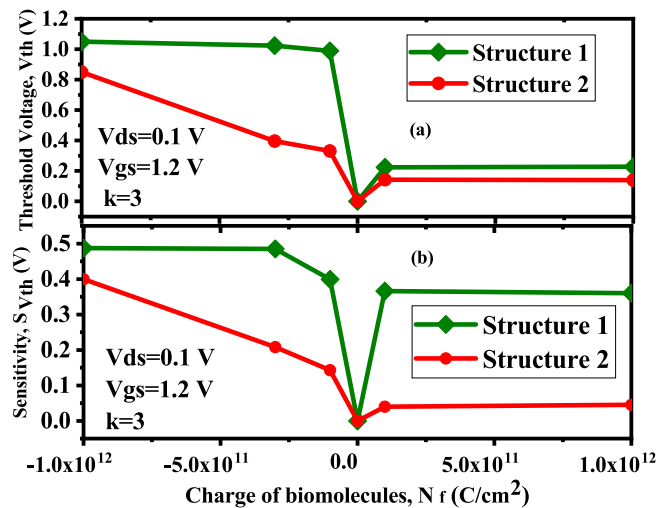


Figure 9. Threshold voltage and Sensitivity w.r.t to negatively and positively charged biomolecules for Device structure-1 and Device structure-2 ($V_{gs} = 1.2$ V, $V_{ds} = 0.1$ V for $\kappa = 3$).

due to biomolecule immobilization leads to a reasonable change in subthreshold current, which is preferable for sensing operation.

Figure 9a,b shows the effect of charged biomolecules on the threshold voltage of the proposed structure. The impact of charged biomolecules on the sensitivity of the device is also depicted in Fig. 9a and b for both the proposed structures. The sensitivity parameter SV_{th} for negatively charged biomolecules in the figure is considerably higher than that for positively charged biomolecules. Additionally, the sensing metric rises in accordance with an increase in the charge density of negatively charged biomolecules. Sensitivity, on the other hand, first show a linear trend with an increase in charge density after that it get saturated to further variations. Before and after immobilising charged molecules, the proposed device's sensitivity can be described as,

$$SV_{th} = \left| \frac{V_{th}(\text{Neutral} - \text{biomolecules}) - V_{th}(\text{Charged} - \text{biomolecules})}{V_{th}(\text{Neutral} - \text{biomolecules})} \right| \quad (3)$$

Since, there is gate over the nano-cavity (Device structure-2) regions, thus, the threshold voltage requirement to deplete the channel will reduce by the amount of V_{fb} compared to Device structure-1 for negatively/positively charged biomolecules, which can be understood from (20). For negatively charged biomolecules the threshold voltage requirement to deplete the channel is more and it is even more for device structure-1 because of the presence of fringing field effects. Which leads to decrement in ON and OFF current for negatively charged biomolecules. Whereas, for positively charged biomolecules, the threshold voltage requirement to deplete the channel is less for both device structures and it is even lesser for Device structure-2 because of the absence of fringing effects. Which leads to increment in ON and OFF current as shown in Fig. 10.

Sensitivity analysis with the variation in thickness and length of the nanogap cavity. In this section we have demonstrated how the device's sensitivity varies with the thickness T_{cav} and length L_{cav} of the cavity. Figure 11a shows the change in threshold voltage SV_{th} with the variation in thickness of the cavity from 7 to 9 nm. With the increase in thickness of the cavity, barrier between source/channel junction increases, results in decrement of the drain current so, as expected V_{th} linearly increases as T_{cav} becomes thicker. The variation in sensitivity parameter with cavity length L_{cav} varying from 30 to 40 nm of channel is shown in Fig. 11b. As the cavity length L_{cav} increases, requirement of threshold voltage increases which leads to low drain current and higher sensitivity, which further improves if the channel length is large as also reported for DM-FET⁶.

Impact of partially filled biomolecules on sensitivity. All of the preceding sections assumed that the cavities were completely filled with biomolecules, but in reality, entirely filled cavities are rarely possible.

Thus, three distinct assumptions of biomolecules filling the nano-cavity are investigated here, as illustrated in Fig. 12. The fill-factor of the nano-cavity is defined as the ratio of the area covered by conjugated biomolecules to the overall area of the nano-cavity in percentage. This section discusses the effect of percentage volume filling of the nano-cavity on the sensitivity of DM-DG-TMD-FET-based biosensor. The fill-factor ($\rho_{T_{bio}}$) defined here as,

$$\rho_{T_{bio}} = \frac{T_{bio}(\text{partially} - \text{filled})}{T_{bio}(\text{fully} - \text{filled})} \times 100 \quad (4)$$

Fill-factor of the completely filled cavity is 100%. For the simulation purpose, L_1 and L_2 are fixed at 35 nm and T_{bio} is taken to be 6 nm for 66% filled cavity and 4 nm for 50% filled cavity and 2 nm for 33% filled cavity. The

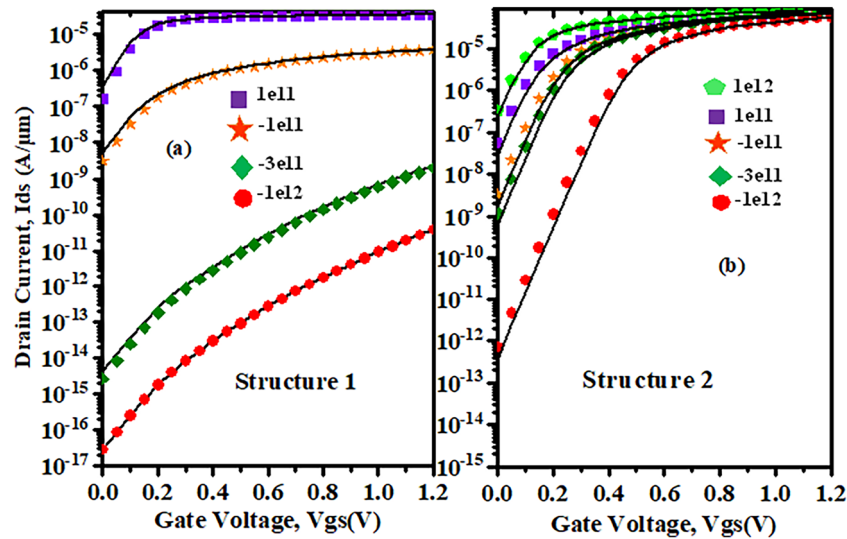


Figure 10. Variation in drain current w.r.t to gate bias for (a) Device structure-1 and (b) Device Structure-2 ($V_{gs} = 1.2$ V $V_{ds} = 0$ V for negatively and positively charged biomolecules for $\kappa = 3$).

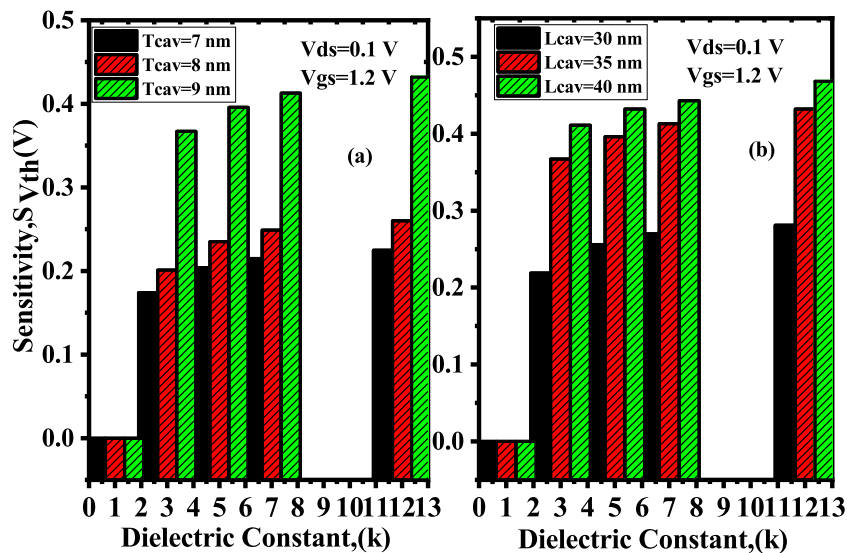


Figure 11. Sensitivity of the device for (a) Variation in cavity thickness (b) Variation cavity length ($V_{gs} = 1, 2$ V, $V_{ds} = 0.1$ V, $\kappa = 5$, $N_f = 1 \times 10^{11}$ C/cm²).

effect of partially filled cavities on the surface potential can be understood through (47) and (48). For different percentage filling of profiles (47) is fed to (24) and (25) for Device structure-1 and for Device structure-2 (48) is used and surface potential for partial filled cavity is calculated using (32) and (33). Figure 13 depicts the surface potential for various assumptions of a filled cavity. The figure shows that as T_{bio} is reduced for non-fully filled cavities, the number of biomolecules inside the cavities decreases and the effective gate capacitance decreases, resulting in less gate control. As a result, the source-to-channel barrier increases. Figure 14 shows the sensitivity for different dielectric constants of biomolecules for the fill in factor of 66%, 50% and 33%.

Sensitivity is observed to enhance with increase in fill-factor from 33% to 100% at a specific value of κ . The maximum sensitivity is shown for a fully filled cavity since the amount of biomolecules conjugation increases as the fill-factor increases. Additionally, it is observed that sensitivity rises as both the fill-factor and the value of κ increase.

Sensitivity analysis due to existence of steric hindrance. Biomolecules are immobilized and hybridized inside the cavity for biosensing operations. Existing hybridized biomolecules block the admission of fresh biomolecules during the process of biomolecule hybridization.

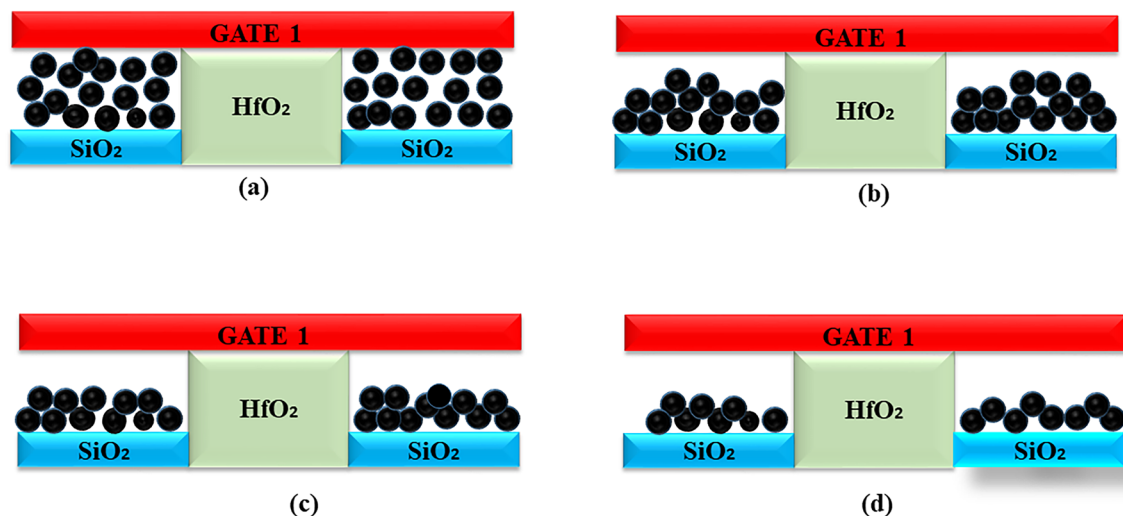


Figure 12. (a) Completely filled cavity (b) 66% filled cavity (c) 50% filled cavity (d) 33% filled cavity.

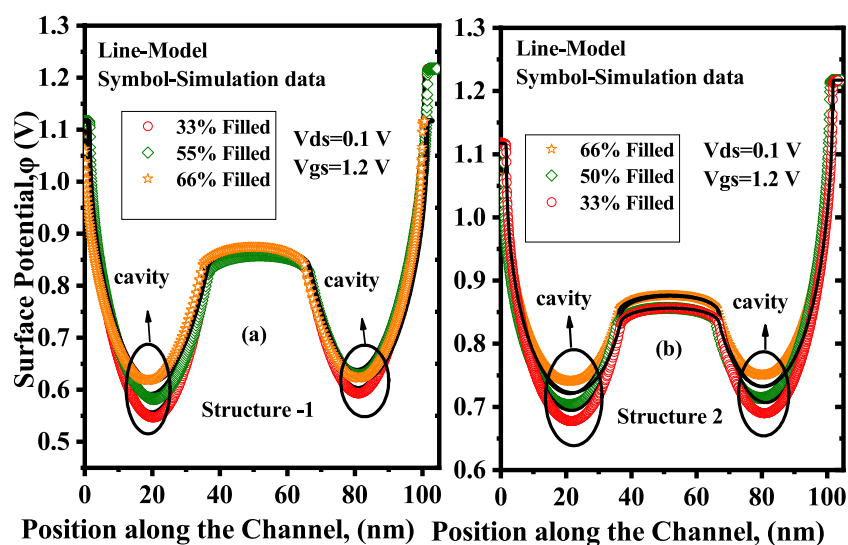


Figure 13. Surface potential of the partially filled cavity (66%,50%,33% filled) ($V_{gs} = 0$ V, $V_{ds} = 0.1$ V, $\kappa = 12$, $N_f = 0$).

This steric hindrance effect may cause biomolecules to hybridize in non-uniform ways along the length of the cavities, according to⁷. Thus, in practical-scenario, completely filled cavities are not conceivable. In this work four different step profiles viz. decreasing, increasing, concave, and convex as shown in Fig. 15a–d to depict the issue of steric hindrance associated with arbitrary and random biomolecular profiles has been considered. A comparison of sensitivities among these profiles has been presented with $\sim 100\%$ filling factor in the cavities. For decreasing step profile, shown in Fig. 15a, biomolecules $\kappa > 1$ will gather nearer to the source/channel junction⁷, and thus coupling between gate and channel enhances. As a consequence, the tunneling rate will speed up and measurable variation on V_{th} happens. Hence, this provide improvement in sensitivity. For the rest of the profiles biomolecules are away from the source to channel interface which reduce the gate to channel coupling and offer poor sensitivities. Decreasing profile of both the structures shows maximum sensitivity. Decreasing profile of Device structure-1 shows sensitivity $S_{V_{th}}$ of 0.789 V while decreasing profiles of Device structure-2 shows 0.28 V of sensitivity as depicted in Fig. 16a,b.

Benchmarking

A large number of biosensors based on analytical modelling and simulation are reported in literature. Here, the sensitivity of monolayer DM-DG-TMD-FET-based biosensor is compared with other reported alternative FET-based biosensors. The estimated sensitivities of FET-based biosensors are extracted from literature and compared with this work. Comparative magnitude of sensitivity metrics form different literature is depicted in Table 2. It

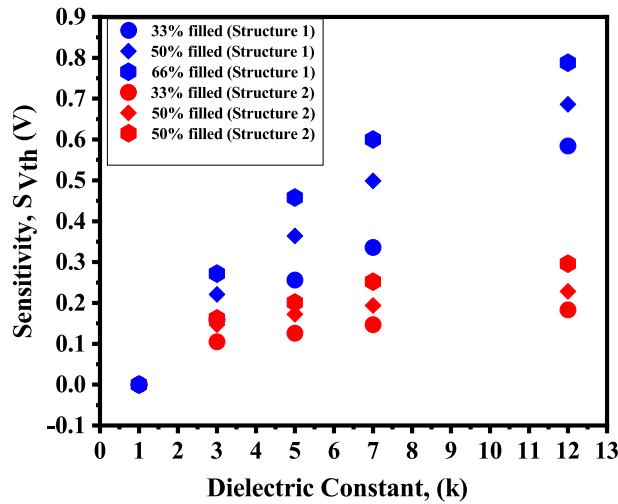


Figure 14. Sensitivity of the proposed DM-DG-TMD-FET-based biosensor when the cavity is partially filled with biomolecules ($V_{gs} = 1.2$ V, $V_{ds} = 0.1$ V).

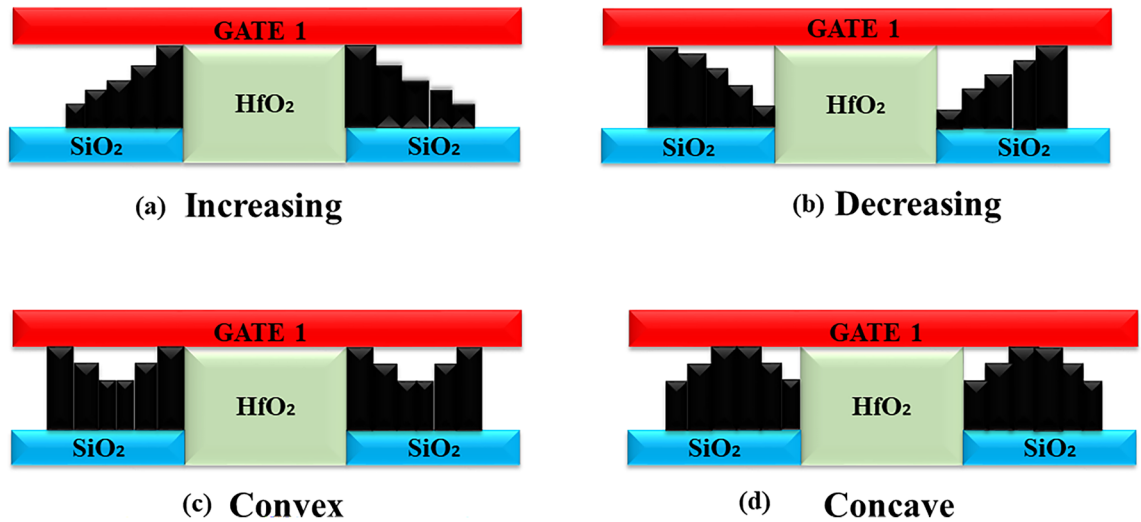


Figure 15. Partially filled cavity profiles (a) Decreasing, (b) Increasing, (c) Convex, and (d) Concave.

is observed from Table 2 that the sensitivity of the proposed Device structure-1 with MoS_2 as channel material shows highest sensitivity among all the FET-based biosensor structures considered for benchmarking purpose. So, it is envisaged that MoS_2 -based proposed Device structure-1 can be a potential candidate for biosensing applications with extremely high sensitivity.

Modelling and simulation methods

In⁴⁰, it is shown that 1-D Poisson’s equation can be a rational approximation to explain the electrostatic behavior in 2-D TMD FETs. Surface potential modelling in this work is also based on the solution of the 1-D Poisson’s equation in the channel⁴⁰. Surface potential distribution $\phi(x)$ in the 2-D channel region can be expressed as,

$$\frac{\delta^2 \Phi_i(x)}{\delta x^2} - P\Phi_i(x) + G = \frac{q}{\epsilon_{ch} T_{ch}} (N_A + n_{2D}(x)) \tag{5}$$

Where ϵ_{tox} and ϵ_{box} are top and bottom gate dielectric constants, respectively. Here T_{tox} and T_{box} are top and bottom gate oxide thicknesses respectively, ϵ_{ch} is the dielectric constant of 2-D material-based channel. N_A is the acceptor type dopant concentration per unit area and $n_{2D}(x)$ is the free inversion carrier concentration. V'_{Gt} and V'_{Gb} are top and bottom gate voltages, respectively defined as,

$$V'_{Gt} = V_{Gt} - V_{Fbt} \tag{6}$$

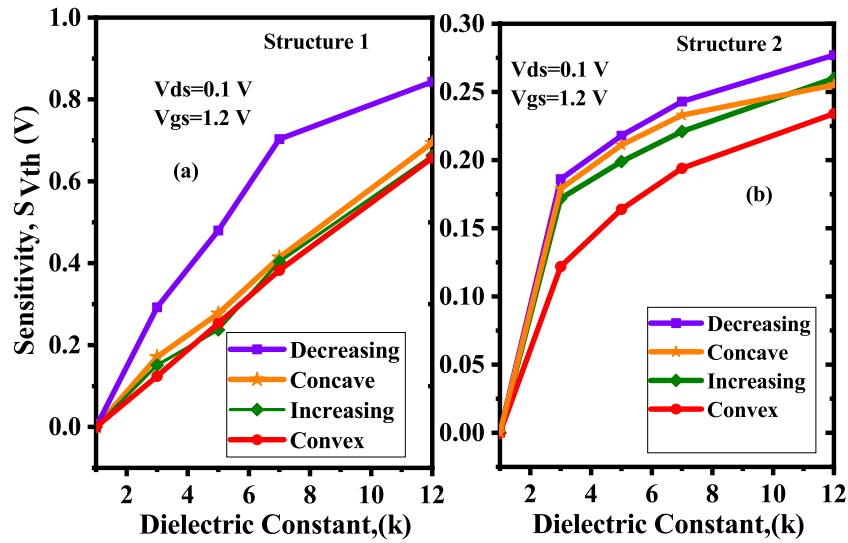


Figure 16. Sensitivity of the proposed DM-DG-TMD-FET-based biosensor for different filling profiles with biomolecules in the cavity ($V_{gs} = 1.2 \text{ V}$, $\kappa = 12$, $N_f=0$).

Reference	Maximum sensitivity of neutral biomolecules (V)	Maximum sensitivity of charged biomolecules (V)
Ref ³²	0.07	0.085
Ref ³³	0.175	-
Ref ³⁴	0.09	0.3
Ref ³¹	0.22	0.35
Ref ³⁵	0.318	-
Ref ³⁶	0.227	0.36
Ref ⁶	0.3	-
Ref ²³	0.1	-
Ref ³⁷	0.2	0.150
Ref ³⁸	0.150	0.45
Ref ³⁹	0.11	-
Ref ⁸	0.8	-
Our work	0.81	0.5

Table 2. Benchmarking with contemporary works of literature.

$$V'_{Bt} = V_{Gt} - V_{Fbb} \tag{7}$$

V_{Fbt} and V_{Fbb} are flat band voltages of top and bottom gate, respectively. where,

$$P = \frac{\epsilon_{tox}}{T_{tox}\epsilon_{ch}T_{ch}} + \frac{\epsilon_{box}}{T_{box}\epsilon_{ch}T_{ch}} \tag{8}$$

$$G = \frac{\epsilon_{tox}}{T_{tox}\epsilon_{ch}T_{ch}}V'_{Gt} + \frac{\epsilon_{box}}{T_{box}}\epsilon_{ch}T_{ch}V'_{Gb} \tag{9}$$

$$n_{2D}(x) = N_{dos}e^{\left(\frac{q}{kT}(\Phi(x)-V(x))\right)} \tag{10}$$

Where N_{dos} is the effective density of states of 2-D channel.

Differentiating (5) with respect to x and substituting the value of $\frac{q}{\epsilon_{ch}T_{ch}}(n_{2D}(x))$ from (5) into the result, we obtain,

$$\frac{\delta^3\Phi_i(x)}{\delta x^3} - P\frac{\delta\Phi_i(x)}{\delta x} = \left(\frac{\delta^2\Phi_i(x)}{\delta x^2} - K\Phi_i(x) + G - \frac{q}{\epsilon_{ch}T_{ch}}N_A\right) \tag{11}$$

The differential equation in (11) cannot be expressed in a closed form analytical solution. Gradual channel approximation is invoked to simplify (11) and equated as $\frac{\delta V}{\delta x} = 0$ ⁴¹. (11) can be simplified further by ignoring

the variations of higher order $\Phi(x)$ with x . As long as the channel is long and drain bias is low, this assumption is valid and it can be expressed as,

$$\frac{\delta\Phi_x}{\delta x} \left(\frac{\delta^2\Phi_i(x)}{\delta x^2} - K\Phi_x + G - \frac{q}{\epsilon_{ch}t_{ch}}N_A + K\frac{kT}{q} \right) = 0 \quad (12)$$

As, lateral electric field is non-zero i.e. $\frac{\delta V}{\delta x} \neq 0$, so, when voltage is applied to the drain, (12) reduces to a linear differential equation as,

$$\frac{\delta^2\Phi_i(x)}{\delta x^2} - K\Phi_i(x) = -A \quad (13)$$

Where,

$$A = \frac{kT}{q}P + \frac{q}{\epsilon_{ch}t_{ch}} + G + N_D \quad (14)$$

The closed form solution of the differential equation in (12) can be expressed as,

$$\Phi(x) = C_1e^{\sqrt{x}} + C_2e^{-\sqrt{x}} + \frac{A_i}{K_i} \quad (15)$$

Modelling of surface potential in overlap region (region II). In the gate overlap channel region i.e. region II (Fig. 1) Surface potential distribution can be expressed as,

$$\Phi_2(x) = C_1e^{\sqrt{x-L_1}} + C_2e^{-\sqrt{x-L_1}} + \frac{A_2}{P_2} \quad (16)$$

Following boundary conditions need to be satisfied in this region for the continuity of potential and electric displacement at the interfaces,

$$A_2 = \frac{kT}{q}K_2 + \frac{q}{\epsilon_{ch}t_{ch}} + G_2 + N_D \quad (17)$$

$$K_2 = \frac{\epsilon_{tox}}{T_{tox}\epsilon_{ch}T_{ch}} + \frac{\epsilon_{box}}{T_{box}\epsilon_{ch}T_{ch}} \quad (18)$$

$$G_2 = \frac{\epsilon_{tox}}{T_{tox}\epsilon_{ch}T_{ch}}V'_{Gt} + \frac{\epsilon_{box}}{T_{box}\epsilon_{ch}T_{ch}}V'_{Gb} \quad (19)$$

Modelling of surface potential in nano-cavity region (region I and region III). In this subsection, detailed modelling of surface potential in the nano-cavity region (Fig. 1) is discussed. Flatband voltage expressions in the nano-cavity regions L_1 and L_3 regions in Fig. 1) can be written as,

$$V_{fb1} = V_{fb3} = V_{fb2} - \frac{qN_f}{C_{eff}} \quad (20)$$

V_{fb1} and V_{fb3} are the flat band voltages of region I and region III, respectively. Here C_{fr} is the gate electrode fringing capacitance. Fringing-field is modeled using the conformal mapping technique, the mapping functions can be expressed as⁴²⁻⁴⁴,

$$(Y - L_G) + j.nX = M.\sinh(v + ju) \quad (21)$$

The structure after transformation of the device and the origin of fringing field is shown in Fig. 17. Now using structural transformation technique⁴²⁻⁴⁴, the fringing capacitance can be expressed as,

$$C_{fr} = \frac{2\epsilon_{bio}}{m\pi L_{1,3}} \sinh \left(\operatorname{acosh} \left(\frac{(T_{ox} - T_{ox1}) + T_g}{T_{ox} - T_{ox1}} \right) \right) \quad (22)$$

Modelling of surface potential in nano-cavity region (region I and region III) for Device structure-1. For the proposed DM-DG-TMD-FET structure-1 mentioned in (Fig. 1a), when the fringing fields are dominant, the effective capacitance is determined primarily by the fringing capacitance.

$$C_{eff} = \frac{C_{ox1}C_{fr}}{C_{ox1} + C_{fr}} \quad (23)$$

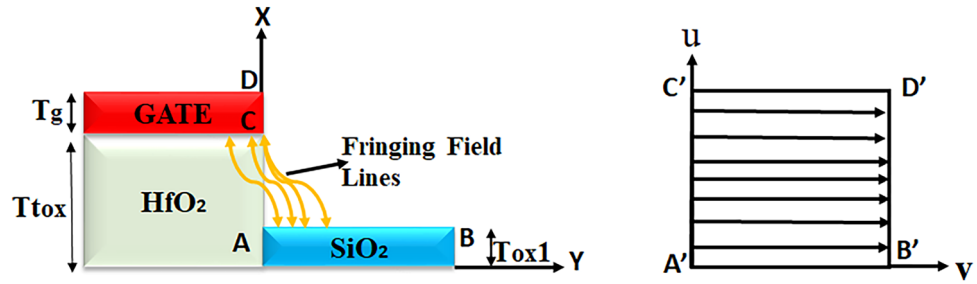


Figure 17. Cross-section of the Device structure 1 (Fig. 1a) showing the fringing field lines and the structural transformation.

So, for the region I (L_1) of the Device structure-1 shown in (Fig. 1a), the closed form expression of surface potential can be written as

$$\Phi_1(x) = C_3e^{\sqrt{x}} + C_4e^{-\sqrt{x}} + \frac{A_1}{P_1} \tag{24}$$

For region III (L_3), the closed form expression of surface potential can be written as,

$$\Phi_3(x) = C_5e^{\sqrt{x-L_1-L_2}} + C_6e^{-\sqrt{x-L_1-L_2}} + \frac{A_3}{P_3} \tag{25}$$

Where,

$$A_1 = \frac{kT}{q}K_1 + \frac{q}{\epsilon_{ch}T_{ch}} + G_1 + N_D \tag{26}$$

$$P_1 = \frac{C_{fr}}{\epsilon_{ch}T_{ch}} + \frac{C_{fr}}{\epsilon_{ch}T_{ch}} \tag{27}$$

$$G_1 = \frac{C_{fr}}{\epsilon_{ch}T_{ch}}V'_{Gt} + \frac{C_{fr}}{\epsilon_{ch}T_{ch}}V'_{Gb} \tag{28}$$

$$A_3 = \frac{kT}{q}K_3 + \frac{q}{\epsilon_{ch}T_{ch}} + G_3 + N_D \tag{29}$$

$$P_3 = \frac{C_{fr}}{\epsilon_{ch}T_{ch}} + \frac{C_{fr}}{\epsilon_{ch}T_{ch}} \tag{30}$$

$$G_3 = \frac{C_{fr}}{\epsilon_{ch}T_{ch}}V'_{Gt} + \frac{C_{eff}}{\epsilon_{ch}T_{ch}}V'_{Gb} \tag{31}$$

Modelling of surface potential in nano-cavity region (region I and region III) for Device structure-2. For region I (L_1) of the Device structure-2 in (Fig. 1b), the closed form expression of surface potential can be written as,

$$\Phi_1(x) = C_3e^{\sqrt{x}} + C_4e^{-\sqrt{x}} + \frac{A_1}{P_1} \tag{32}$$

For region III (L_3), the closed form expression of surface potential can be written as,

$$\Phi_3(x) = C_5e^{\sqrt{x-L_1-L_2}} + C_6e^{-\sqrt{x-L_1-L_2}} + \frac{A_3}{P_3} \tag{33}$$

Where,

$$A_1 = \frac{kT}{q}K_1 + \frac{q}{\epsilon_{ch}t_{ch}} + G_1 + N_D \tag{34}$$

$$P_1 = \frac{C_{eff}}{\varepsilon_{ch}T_{ch}} + \frac{C_{eff}}{\varepsilon_{ch}T_{ch}} \quad (35)$$

$$G_1 = \frac{C_{eff}}{\varepsilon_{ch}T_{ch}} V'_{Gt} + \frac{C_{eff}}{\varepsilon_{ch}T_{ch}} V'_{Gb} \quad (36)$$

$$A_3 = \frac{kT}{q} K_3 + \frac{q}{\varepsilon_{ch}T_{ch}} + G_3 + N_D \quad (37)$$

$$P_3 = \frac{C_{eff}}{\varepsilon_{ch}T_{ch}} + \frac{C_{eff}}{\varepsilon_{ch}T_{ch}} \quad (38)$$

$$G_3 = \frac{C_{eff}}{\varepsilon_{ch}T_{ch}} V'_{Gt} + \frac{C_{eff}}{\varepsilon_{ch}T_{ch}} V'_{Gb} \quad (39)$$

For the proposed DM-DG-TMD-FET structure-2 mentioned in (Fig. 1b), when the fringing fields are less dominant, the effective capacitance is determined primarily by the gate capacitance.

$$C_{eff} = \frac{C_{ox1}C_{gap}}{C_{ox1} + C_{gap}} \quad (40)$$

Here, C_{gap} is the capacitance of cavity region and it can be expressed as, $(\frac{\varepsilon_{bio}}{T_{cav}})$. For finding out the constant coefficients, C_1, C_2, C_3, C_4, C_5 and, C_6 , following boundary conditions are enforced.

$$\Phi_1(x=0) = V_s + V_{bi} + \frac{KT}{q} \ln\left(\frac{N_{sd}}{N_{dos}}\right) \quad (41)$$

$$\Phi_1(x=L_1) = \Phi_2(x=L_1) \quad (42)$$

$$\frac{\delta\Phi_1(x)}{\delta x} = \frac{\delta\Phi_2(x)}{\delta x} \text{ at } (x=L_1) \quad (43)$$

$$\Phi_2(x=L_2) = \Phi_3(x=L_2) \quad (44)$$

$$\frac{\delta\Phi_2(x)}{\delta x} = \frac{\delta\Phi_3(x)}{\delta x} \text{ at } (x=L_2) \quad (45)$$

$$\Phi_3(x=L_3) = V_d + V_{bi} + \frac{KT}{q} \ln\left(\frac{N_{sd}}{N_{dos}}\right) \quad (46)$$

Solving (42), (43), (44) and, (45), the constant coefficients can be evaluated and then substituting the values of constants in (24), (25), (32) and (33) surface potential can be evaluated.

Surface potential modelling for partially filled cavity. In this section, surface potential is modeled for the mentioned device structures in (Fig. 1) with partially filled nano-cavity which is filled upto a certain height, T_{bio} . For Device structure-1 (Fig. 1a) $T_{cav}=T_{bio}$ considered as 10 nm and for Device structure-2 (Fig. 1b) as 9 nm (this is for fully filled case). For partially field case, T_{bio} can be treated as a parameter. Gate electrode fringing capacitance when the nano-cavity of region I and region III is partially filled upto a certain height (T_{bio}) can be expressed as,

$$C_{fr} = \frac{2\varepsilon_{bio}}{m\pi L_{1,3}} \sinh\left(\text{acosh}\left(\frac{(EOT - T_{ox} - T_{ox1}) + T_g}{EOT - T_{ox} - T_{ox1}}\right)\right) \quad (47)$$

Where

$$EOT = T_{bio} + \frac{\varepsilon_{bio}}{\varepsilon_{air}}(T_{cav} - T_{bio}) \quad (48)$$

where T_{bio} is the height of biomolecules occupancy and ε_{bio} is the dielectric constant of biomolecules. By substituting (47) in (24) and in (25) surface potential for partially cavity case can be obtained. For the proposed Device structure-2, effect of (48) will get added to (40) and from (32) and (33), surface potential for partially filled cavity case can be obtained.

Drain current modelling. Model of drain current in subthreshold region is calculated by utilizing expressions of surface potential obtained in previous section⁴⁵ and can be expressed as,

$$I_{dsub} = \frac{\mu WkT \frac{N_{dos}^2}{N_{dos}} \left(1 - e^{-\frac{qV_{ds}}{kT}} \right)}{\sum_{i=1}^3 \int_0^{L_i} e^{\frac{q\Phi_i(x)}{kT}} dx} \quad (49)$$

For linear regime, three transistor modelling approach has been employed to calculate the drain current⁴⁶. Both the subthreshold current and linear regime current have been equated at transition region for the continuity of the current. The carrier transport is governed by the drift-diffusion equation described as,

$$I_{ds} = qWn_{2D}(x)\mu(x) \frac{\delta V(x)}{\delta x} \quad (50)$$

Where $\mu(x)$ is carrier mobility in the channel, and W is device width. Here an extraction of $V(x)$ in terms of x to calculate the drain current is required. We assume a linear profile of $V(x)$ and simplified expression of potential can be written as

$$V(x) = M(x) + C \quad (51)$$

The constants M and C can be evaluated as mentioned in²³. To incorporate the effect of gate bias, an empirical fitting function $F(V_G)$ can be considered with C . So, the final form of C can be expressed as,

$$C = V_s + V_{bi} + F(V_G) \quad (52)$$

Now integrating (50) w.r.t to x , current in each region can be evaluated. The drain current in region I,II,III (Fig. 1) is the drain current of the DM-DG-TMD-FET with channel length, L_1 , L_2 , and L_3 respectively, and it can be expressed as,

$$I_{dlinear,i} = \frac{q\mu_n N_{dos}}{L_i} \int_0^{L_i} \exp\left(\frac{q}{kT}(\Phi_i(x) + \frac{A}{K} - Mx - C)\right) dx \quad (53)$$

Where, $i = 1, 2, 3$.

Simulation methodology. The developed model of the TMD FET-based biosensor has been validated with the 2-dimensional numeric simulator SILVACO TCAD²⁵. Atomistic simulators such as Nano TCAD ViDES is compatible for atomistics simulations of TMD devices but they suffer from computational complexity and it has its own limitations. Moreover, many recent work based 2-D materials FET have been using SILVACO TCAD for simulating FETs^{18,47}. In SILVACO TCAD, while defining 2-D materials, the electrical properties of materials like permittivity, density of states, electron and hole effective masses, affinity, electron and hole mobilities need to be defined. For simulation of the proposed device we have adopted the fermi-dirac carrier distribution, the electric field-dependent mobility (FLDMOB) model concentration dependent mobility (CONMOB) model. Shockley-Read-Hall recombination model is also included for the recombination mechanism. As the source and drain regions are highly doped regions, a significant amount of band bending is there in these regions due to high doping, to include this in calculations, Band-gap narrowing model(BGN) has also been considered. The effect of neutral biomolecules is modeled by introducing a dielectric materials having dielectric constant (κ) varied between 1 to 12, which lies in the range of dielectric constant of different biomolecules (e.g., Protein ($\kappa = 2.50$), Biotin ($\kappa = 2.63$), APTES ($\kappa = 3.57$), Protein ($\kappa = 6$) and Streptavidin ($\kappa = 2.1$)^{5,48}). Negative and positive charge density ($N_f = -1 \times 10^{-12} \text{ C/m}^2$ to $+1 \times 10^{11} \text{ C/m}^2$) at the $\text{MoS}_2/\text{SiO}_2$ interface is considered to model the impact of charged biomolecules. Material parameters of the TMD materials have been extracted from⁴⁷.

Conclusion

In this work, for monolayer MoS_2 -based dual-gate FET-based biosensor, an analytical model has been developed including the fringing-field effect. The model is developed in such a way that it can be utilized to design DM-DG-TMD FET-based biosensor based on the principle of modulation of dielectric constants. The proposed model can be applied to any TMD material to measure its impact on sensitivity. The proposed biosensor shows $\sim 100\%$ higher sensitivity in Device structure-1 compared to Device structure-2. Channel surface potential and transfer characteristics obtained from the model show a quantifiable variation in sensor output with the variation of dielectric constant in the nano-cavity region. The effect of partially filled cavities has been also modeled and investigated in this work. Steric hindrance issue has also been studied in this work. The results demonstrate that the completely filled cavity shows $\sim 92\%$ higher sensitivity than the partially filled cavities (i.e. 33% filled cavity). Optimization of device dimensions has also been done to enhance the sensitivity of the proposed biosensors. Finally, benchmarking of the proposed biosensor is presented with contemporary, state of the art biosensors and it is highlighted that MoS_2 FET-based biosensor emerges with a superior sensitivity $S_{V_{th}} = 0.81 \text{ V}$ for $\kappa = 12$. Finally, it is concluded that our proposed DM-DG-TMD FET-based Biosensor structure-1 model is an extremely promising candidate for the biosensing applications due to its enhanced sensitivity and label-free detection trait which could be immensely useful for detection of lower concentration of biomolecules.

Data availability

Data can be available upon reasonable request to the corresponding author.

References

- Gu, B. *et al.* Nanogap field-effect transistor biosensors for electrical detection of avian influenza. *Small (Weinheim an der Bergstrasse, Germany)* **5**(21), 2407–2412. <https://doi.org/10.1002/sml.200900450> (2009).
- Im, H., Huang, X. J., Gu, B. & Choi, Y. K. A dielectric-modulated field-effect transistor for biosensing. *Nat. Nanotechnol.* **2**(7), 430–434. <https://doi.org/10.1038/nnano.2007.180> (2007).
- Lee, K.-W. *et al.* An underlap field-effect transistor for electrical detection of influenza. *Appl. Phys. Lett.* **96**, 033703 (2010).
- Okay, A. K. *et al.* Using nanogap in label-free impedance based electrical biosensors to overcome electrical double layer effect. *Microsyst. Technol.-Micro- Nanosyst.-Inf. Storage Process. Syst.* **23**(4), 889–897. <https://doi.org/10.1007/s00542-015-2764-4> (2017).
- Narang, R., Reddy, K. S., Saxena, M., Gupta, R. S. & Gupta, M. A dielectric-modulated tunnel-FET-based biosensor for label-free detection: Analytical modelling study and sensitivity analysis. *IEEE Trans. Electron Devices* **59**(10), 2809–2817. <https://doi.org/10.1109/TED.2012.2208115> (2012).
- Maji, M. & Saini, G. Modelling of dual material surrounding split gate junctionless transistor as biosensor. *Superlattices Microstruct.* **135**, 106290 (2019).
- Bhattacharyya, A., Chanda, M. & De, D. Analysis of partial hybridization and probe positioning on sensitivity of a dielectric modulated junctionless label free biosensor. *IEEE Trans. Nanotechnol.* **19**, 719–727. <https://doi.org/10.1109/TNANO.2020.3025544> (2020).
- Narang, R., Saxena, M. & Gupta, M. Comparative analysis of dielectric modulated FET and TFET-based biosensor. *IEEE Trans. Nanotechnol.* **14**(3), 427–435 (2015).
- Kim, *et al.* A new sensing metric to reduce data fluctuations in a nanogap-embedded field-effect transistor biosensor. *IEEE Trans. Electron Devices* **59**(10), 2825–2831. <https://doi.org/10.1109/TED.2012.2209650> (2012).
- Park, H. *et al.* Label-free and recalibrated multilayer MoS₂ biosensor for point-of-care diagnostics. *ACS Appl. Mater. Interfaces* **9**(50), 43490–43497. <https://doi.org/10.1021/acsami.7b14479> (2017).
- Pumera, M. & Loo, A. H. Layered transition-metal dichalcogenides (MoS₂ and WS₂) for sensing and biosensing. *TrAC Trends Anal. Chem.* **61**, 49–53. <https://doi.org/10.1016/j.trac.2014.05.009> (2014).
- Sarkar, D. *et al.* MoS₂ Field-Effect Transistor for Next-Generation Label-Free Biosensors. *ACS Nano*. **8**(4), 3992–4003 (2014).
- Masurkar, N., Varma, S. & Mohana Reddy Arava, L. Supported and suspended 2D material-based FET biosensors. *Electrochem* **1**, 260–277. <https://doi.org/10.3390/electrochem1030017> (2020).
- Lee, J. *et al.* Two-dimensional layered MoS₂ biosensors enable highly sensitive detection of biomolecules. *Sci. Rep.* **4**, 7352. <https://doi.org/10.1038/srep07352> (2015).
- Wen, W. *et al.* Recent advances in emerging 2-D nanomaterials for biosensing and bioimaging applications. *Mater. Today* **21**(2), 164–177 (2018).
- Gan, X., Zhao, H. & Quan, X. Two-dimensional MoS₂: A promising building block for biosensors. *Biosens. Bioelectron.* **89**, 56–71. <https://doi.org/10.1016/j.bios.2016.03.042> (2017).
- Alam, K. & Lake, R. K. Monolayer MoS₂ transistors beyond the technology road map. *IEEE Trans. Electron Devices* **59**(12), 3250–3254 (2012).
- Ilatikhameneh, *et al.* Tunnel field-effect transistors in 2-D transition metal dichalcogenide materials. *IEEE J. Explor. Solid-State Comput. Devices Circuits* **1**, 12–18. <https://doi.org/10.1109/JXCDC.2015.2423096> (2015).
- Rahman, E., Shadman, A., Ahmed, I., Khan, S. Z. & Khosru, Q. D. M. Monolayer MoS₂ and WSe₂ double gate field effect transistor as super Nernst pH sensor and nanobiosensor. *Sens. Bio-Sens. Res.* **11**(1), 45–51 (2016).
- Jawaid, A. *et al.* Mechanism for liquid phase exfoliation of MoS₂. *Chem. Mater.* **28**, 337–348. <https://doi.org/10.1021/acs.chemmater.5b04224> (2016).
- Wang, *et al.* Functionalized MoS₂ nanosheet-based field-effect biosensor for label-free sensitive detection of cancer marker proteins in solution. *Small (Weinheim an der Bergstrasse, Germany)* **10**(6), 1101–1105. <https://doi.org/10.1002/sml.201302081> (2014).
- Nam, H. *et al.* Two different device physics principles for operating MoS₂ transistor biosensors with femtomolar-level detection limits. *Appl. Phys. Lett.* **107**(1), 012105 (2015).
- Rahman, E., Shadman, A., Ahmed, I., Khan, S. Z. & Khosru, Q. D. M. A physically based compact I-V model for monolayer TMDC channel MOSFET and DMFET biosensor. *Nanotechnology* **29**(23), 235203 (2018).
- Fang, H. *et al.* High-performance single layered WSe₂ p-FETs with chemically doped contacts. *Nano Lett.* **12**(7), 3788–3792 (2012).
- ATLAS User's Manual. (Silvaco IncA, 2015).
- Masurkar, *et al.* Reliable and highly sensitive biosensor from suspended MoS₂ atomic layer on nanogap electrodes. *Biosens. Bioelectron. Retrieved* **172**, 112724. <https://doi.org/10.1016/j.bios.2020.112724> (2021).
- Rawat, *et al.* Two-dimensional MoS₂-based electrochemical biosensor for highly selective detection of glutathione. *IEEE Sens. J.* **20**(13), 6937–6944. <https://doi.org/10.1109/JSEN.2020.2978275> (2020).
- Rawat, B., Vinaya, M. M. & Paily, R. Transition metal dichalcogenide-based field-effect transistors for analog/mixed-signal applications. *IEEE Trans. Electron Devices* **66**(5), 2424–2430. <https://doi.org/10.1109/TED.2019.2906235> (2019).
- Nam, H. *et al.* Fabrication and comparison of MoS₂ and WSe₂ field-effect transistor biosensors. *J. Vacuum Sci. Technol. B Nanotechnol. Microelectron. Mater. Process. Meas. Phenomena* **33**(6), 06FG01. <https://doi.org/10.1116/1.4930040> (2015).
- Tsividis, Y. & McAndrew, C. *Operation and Modelling of the MOS Transistor* 2nd edn. (Oxford University, 2011).
- Singh, S. & Raja, B. Analytical modelling of split-gate junction-less transistor for a biosensor application. *Sens. Bio-Sens. Res.* **18**, 31–36 (2018).
- Kumari, M. *et al.* Work function optimization for enhancement of sensitivity of dual-material (DM), double-gate (DG), junctionless MOSFET-based biosensor. *Appl. Phys. A* **127**, 130. <https://doi.org/10.1007/s00339-020-04256-0> (2021).
- Chakraborty, A. & Sarkar, A. Analytical modelling and sensitivity analysis of dielectric-modulated junctionless gate stack surrounding gate MOSFET (JLGSSRG) for application as biosensor. *J. Comput. Electron* **16**, 556–567. <https://doi.org/10.1007/s10825-017-0999-2> (2017).
- Narang, R., Saxena, M. & Gupta, M. Investigation of dielectric modulated (DM) double gate (DG) junctionless MOSFETs for application as a biosensors. *Superlattices Microstruct.* **85**, 557–572 (2015).
- Das, R. *et al.* Analytical modelling of sensitivity parameters influenced by practically feasible arrangement of bio-molecules in dielectric modulated FET biosensor. *Silicon* <https://doi.org/10.1007/s12633-021-01617-z> (2022).
- Kumari, M., Singh, N. K., Sahoo, M. & Rahaman, H. 2-D analytical modelling and simulation of dual material, double gate, gate stack engineered, junctionless MOSFET based biosensor with enhanced sensitivity. *Silicon* <https://doi.org/10.1007/s12633-021-01223-z> (2021).
- Maiti, S., De, A. & Sarkar, S. K. Analytical modelling of symmetric gate underlap quadruple gate multichannel junctionless MOSFET biosensor. *Silicon* <https://doi.org/10.1007/s12633-021-01415-7> (2021).
- Singh, K. N. & Dutta, P. K. Analytical modelling of a high-K underlap dielectric- and charge-modulated silicon-on-nothing FET based biosensor. *J. Comput. Electron.* **19**, 1126–1135. <https://doi.org/10.1007/s10825-020-01511-8> (2020).

39. Parija, S. K. *et al.* Comparison study of DG MOSFET with and without gate stack configuration for biosensor applications. *Silicon* <https://doi.org/10.1007/s12633-021-01118-z> (2021).
40. Cao, W., Kang, J., Liu, W. & Banerjee, K. A compact current-voltage model for 2D semiconductor based field-effect transistors considering interface traps, mobility degradation, and inefficient doping effect. *IEEE Trans. Electron Devices* **61**(12), 4282–4290 (2014).
41. Jimenez, D., Miranda, E. & Godoy, A. Analytic model for the surface potential and drain current in negative capacitance field-effect transistors. *IEEE Trans. Electron Devices* **57**(10), 2405–2409 (2010).
42. Bansal, A., Paul, B. C. & Roy, K. Modelling and optimization of fringe capacitance of nanoscale DG MOS devices. *IEEE Trans. Electron Devices* **52**(2), 256–262. <https://doi.org/10.1109/TED.2004.842713> (2005).
43. Mohapatra, N. R., Desai, M. P., Narendra, S. G. & Ramgopal Rao, V. Modelling of parasitic capacitances in deep submicrometer conventional and high-K dielectric MOS transistors. *IEEE Trans. Electron Devices* **50**(4), 959–966. <https://doi.org/10.1109/TED.2003.811387> (2003).
44. Lin, S. C. & Kuo, J. B. Modelling the fringing electric field effect on the threshold voltage of FD SOI nMOS devices with the LDD/sidewall oxide spacer structure. *IEEE Trans. Electron Devices* **50**(12), 2559–2564. <https://doi.org/10.1109/TED.2003.816910> (2003).
45. Francis, P., Terao, A., Flandre, D. & Van de Wiele, F. Modelling of ultrathin double-gate nMOS/SOI transistors. *IEEE Trans. Electron Devices* **41**(5), 715–719 (1994).
46. Razavi, P. & Orouji, A. A. Nanoscale triple material double gate (TMDG) MOSFET for improving short channel effects. In *Proc. ICAE*, 11–14 (2008).
47. Singh, N. K. & Sahoo, M. Analytical modelling of short-channel TMD TFET considering effect of fringing field and 2-D junctions depletion regions. *IEEE Trans. Electron Devices* **69**(2), 843–850 (2022).
48. Morgan, H., Taylor, D. M. & D'Silva, C. Surface plasmon resonance studies of chemisorbed biotin-streptavidin multilayers. *Thin Solid Films* **209**(1), 122–126 (1992).

Author contributions

The idea was formulated by M.K. and M.S. M.K. did the simulation and modelling. This paper's technical analysis was developed by M.K. and N.K.S. All three authors contributed equally to the writing. M.K. and M.S. completed the manuscript's finalization.

Competing interests

The authors declare no competing interests.

Additional information

Correspondence and requests for materials should be addressed to M.S.

Reprints and permissions information is available at www.nature.com/reprints.

Publisher's note Springer Nature remains neutral with regard to jurisdictional claims in published maps and institutional affiliations.



Open Access This article is licensed under a Creative Commons Attribution 4.0 International License, which permits use, sharing, adaptation, distribution and reproduction in any medium or format, as long as you give appropriate credit to the original author(s) and the source, provide a link to the Creative Commons licence, and indicate if changes were made. The images or other third party material in this article are included in the article's Creative Commons licence, unless indicated otherwise in a credit line to the material. If material is not included in the article's Creative Commons licence and your intended use is not permitted by statutory regulation or exceeds the permitted use, you will need to obtain permission directly from the copyright holder. To view a copy of this licence, visit <http://creativecommons.org/licenses/by/4.0/>.

© The Author(s) 2022